Electronic Supplementary Material (ESI) for Journal of Materials Chemistry A.

Supplementary Information

Enhancing Polysulfides Confining and Converting in Meso-/microporous MoC/NC Microspheres for Lithium-Sulfur Batteries

Wanli Li,[†a] Xiangfeng Jin,[†b] Liangping Xiao,[c] Xingyun Li,[a] Qingchi Xu,[*,c] Jian Weng[*,a] and Jun Xu[*c,d]

[a] *Department of Biomaterials, College of Materials, Xiamen University, Xiamen 361005, Fujian, China.*
[b] *Department of Chemistry, College of Chemistry and Chemical Engineering, Xiamen University, Xiamen 361005, Fujian, China.*
[c] *Department of Physics, Research Institute for Biomimetics and Soft Matter, Fujian Provincial Key Laboratory for Soft Functional Materials, Xiamen University, Xiamen 361005, Fujian, China.*
[d] *Shenzhen Research Institute of Xiamen University, Shenzhen 518057, Guangdong, China.*

† These authors contributed equally to this work.

Experimental

Preparation of cathode materials

Synthesis of Mo-polydopamine (Mo-PDA) microspheres. The Mo-glycerate (MoG) solid microspheres were prepared according to the literature.[1] Then 8 mg of MoG and 8 mg of dopamine hydrochloride were dispersed into a mixed solvent containing 7.5 mL of methanol and 5 mL of H_2O. The mixture was stirred for 10 min and sonicated for 10 min to obtain a uniform dispersion. Subsequently, 15 μL of $NH_3 \cdot H_2O$ was added to the mixture dropwise and stirred vigorously. Then the mixture was stirred gently for 24 h at 20 ºC. Finally, the brownish-black product was collected by centrifugation at 9000 rpm for 10 min, washed three times with H_2O and ethanol (EtOH), and dried in a vacuum oven at 60 ºC overnight. Then the Mo-PDA core-shelled microspheres (Mo-PDA CSMSs) were obtained. As for comparisons, the Mo-PDA hollow microspheres (Mo-PDA HMSs) were obtained according to the literature,[1] when the content of $NH_3 \cdot H_2O$ was increased to 40 μL, and the mixture was transferred to a Teflon-lined stainless steel autoclave and kept at 140 ºC for 2 h.

Synthesis of MoC/NC microspheres. The as-synthesized Mo-PDA CSMSs were thermally treated at 800 ºC for 8 h with a heating rate of 5 ºC min^{-1} under Ar/H_2 (95:5, volume ratio) atmosphere, and the gas flow rate was controlled below 20 mL min^{-1}. The final MoC/NC CSMSs were obtained. It should be noted that the heating rate of MoC/NC hollow microspheres (MoC/NC HMSs) was 1 ºC min^{-1}, to keep the stability of hollow structures. The N-doped carbon-based core-shelled microspheres (NC CSMSs) were obtained by etching MoC nanocrystals in the MoC/NC CSMSs with 2 wt% $NH_3 \cdot H_2O$ and a certain amount of H_2O_2 additive. The MoC/NC nanoparticles (MoC/NC NPs) were formed when the treatment temperature is 900 ºC.

Synthesis of MoC/NC/S composites. The MoC/NC/S composites were prepared by a typical melt diffusion method. The as-synthesized MoC/NC CSMSs, NC CSMSs or MoC/NC HMSs were mixed with sublimed sulfur (1:3, weight ratio), respectively, and heated at 155 ºC in a sealed container for 15 h, then continued with heat treatment of 160 ºC for 6 h in an opened glass bottle to remove extra sulfur.

Material Characterizations

The morphologies, microstructures, and elemental mapping analyses were performed by using a field-emission scanning electron microscope (FESEM, SU-70, Hitachi) at an acceleration voltage from 5 to 20 kV, transmission electron microscopy (TEM, JEM-2100, 200 kV), and field-emission transmission electron microscope (STEM, Talos F200, FEI, 200 kV). The crystal structures were analyzed by using X-ray powder diffraction (XRD, Bruker, Cu Kα radiation, 40 kV, 40 mA). The graphitic degree of carbon in products was recorded by Raman spectra (XploRA, HORIBA, Jobin-Yvon, 532 nm). Thermogravimetric analysis (TGA, NETZSCH TG 209 F1) was performed in a flow of air or N_2 with a heating rate of 10 ºC min^{-1}. X-ray photoelectron spectroscopy (XPS, Escalab 250 Xi, Al Kα, Thermo Fisher) was used to analyze the chemical and electronic state of the surface. The quantitative elemental analysis based on CHN model were performed to calculate the percentage of C and N element in the sample. The specific surface areas and pore size distributions of the products were examined by the N_2 adsorption-desorption isotherms (ASAP 2460) at liquid-nitrogen temperature (78 K). The surface area was calculated by the Brunauer-Emmett-Teller (BET) method, the DFT Model was used in the calculation of pore size distributions. Besides, the residual lithium polysulfides (LiPSs) in 1,3-dioxolane (DOL) and 1,2-dimethoxyethane (DME) (1:1, volume ratio) solution was determined by an ultraviolet-visible (UV-vis) spectrophotometer (UV-2550, Shimadzu) with a wavelength range from 300 to 800 nm.

Electrochemical characterization

The electrochemical performance of the prepared samples was investigated by assembling 2032-type coin cells in an Ar-filled glove box, which consisted of a cathode with active materials, separator, Li anode, and liquid electrolyte. The cathodes were fabricated by mixing 75 wt% active material (MoC/NC/S CSMSs, NC/S CSMSs, or MoC/NC/S HMSs), 15 wt% conducting additive (ketjen black), and 10 wt% binders (LA 133), and stirred for 10 h with the aid of a certain amount of H_2O and EtOH to obtain a homogeneous slurry. Then the slurry was coated on the Al foil (current collector) using a mini tape casting coater (MSK-AFA-HC100, MTI). After being dried at 60 ºC for 12 h under vacuum, the electrodes were punched into 1.2 cm disks using a disc cutter (MSK-T-10, MTI) with low sulfur loading 1.0 to 1.5 mg cm^{-2}. While the electrodes of high sulfur loading ~ 5mg cm^{-2} were fabricated with commercial carbon cloth (CC, WOS1009) as the current collector. The area of each sulfur cathode is controlled at 1.13 cm^{-2}. The Celgard 2500 was used as the separator. The electrolyte was 1 M lithium bis(trifluoromethanesulfonyl)imide (LiTFSI) in DOL/DME (1:1, volume ratio) solution with 2 wt% $LiNO_3$ additive. The commercial Li metal foil, with an area of 1.91 cm^{-2} and thickness of 450 μm, is used as an anode. Whereupon, the negative/positive (N/P) ratio is calculated to be

55.4 to 36.9 for the low-areal sulfur loadings, and 11.1 for the high-areal sulfur loadings. The electrolyte/sulfur (E/S) ratio was 20 μL mg^{-1} for the low sulfur loadings, and 10 μL mg^{-1} for the high sulfur loadings. Cyclic voltammetry (CV, CHI440C) measurements were carried out at a scan rate of 0.1 to 1 mV s^{-1} between 1.7 and 2.8 V (vs. Li^+/Li), and electrochemical impedance spectra (EIS, Zennium, Zahner) were measured in the frequency range of 100 kHz to 0.1 Hz with an AC amplitude of 5 mV. Galvanostatic discharge/charge measurements were performed with a battery testing system (LAND CT2001A) at 25 ºC in the voltage range of 1.8 to 2.7 V with different current rates from 0.1 to 5 C (1 C = 1675 mA g^{-1}). All of the capacities were calculated based on the mass of sulfur.

Time-dependent absorbance test

The adsorption kinetics of the MoC/NC CSMSs for the Li_2S_8 trapping was measured by UV-vis absorption spectrophotometry. To demonstrate the important role of the outer shells for the LiPSs trapping, the MoC/NC CSMSs with broken outer shells were prepared as a contrast, which was obtained by sonication with a cell crusher at 760 W for 5 h. First, the Li_2S_8 solution was prepared as follow: 0.069 g of Li_2S and 0.32 g of sulfur were dissolved in a 5 mL mixture solvent of DOL/DME (1:1, volume ratio) and stirred at 80 ºC for 24 h inside an argon-filled glove box, the 0.3 M Li_2S_8 solution was synthesized. Second, 10 mg of the two types of MoC/NC CSMSs powders were soaked in 2.5 mL of Li_2S_8 solution (diluted to 1.5 mM) for 10 h, respectively. The absorbance curves of the solutions were measured after 30 min for most of the powders sedimentation. As Li_2S_8 was continuously captured by the MoC/NC powders, the detailed absorbance changes at 410 nm were recorded every 30 min.

Li_2S_6 Adsorption test

The synthetic process of the Li_2S_6 solution was the same as the previous process of preparing the Li_2S_8 solution, except for the content of sulfur that was changed to 0.24 g. Then 10 mg of MoC/NC CSMSs, NC CSMSs, and MoC/NC NPs were added into 2.5 mL of Li_2S_6 solution (diluted to 3 mM), respectively. After 12 h rest, the photograph of visualized adsorption was obtained, and the concentration of residual LiPSs in the solution was determined by UV-vis spectra.

Symmetrical cell assembly and measurements

The MoC/NC CSMSs, NC CSMSs, or MoC/NC NPs were mixed with the LA133 binder with a weight ratio of 4:1, respectively. After stirring for 12 h with the aid of a certain amount of EtOH and H_2O, the obtained homogenous slurry was coated onto the Al foil and dried at 60 ºC for 12 h under vacuum. Then the electrodes were punched into 1.2 cm disks, and the mass loadings of active materials were about 1 mg cm^{-2}. Next, two identical electrodes were assembled to a standard 2025 coin cell with a Clegard 2500 polypropylene membrane as the separator. 40 μL electrolyte containing 0.3 M Li_2S_6 and 1 M LiTFSI in a mixed solvent of DOL/DME (1:1, volume ratio) was added into each cell. CV measurements were performed at a scan rate of 2 mV s^{-1} between -1 and 1 V.

Density functional theory (DFT) calculations

The first-principles calculations were performed using DFT as implemented in the Vienna Ab initio Simulation Package (VASP) with the exchange-correlation function of Perdew-Burke-Ernzerhof. The electron-ion interaction was considered in the form of the projector augmented wave (PAW) approach. Energy cutoff of 500 eV for the plane-wave basis set was used for the structure optimization and transition states search.[2-4] A supercell model of MoC with a 2×2 surface and six layers was used for the calculations, which includes 27 Mo atoms and 27 carbon atoms in total. Brillouin k-point meshes of 3×3×1 for MoC (111) and 2×2×1 for graphene were generated. The total energy convergence and the forces on each atom were set to be lower than 10^{-5} eV and 0.05 eV A^{-1}. The adsorption energy (E_{ads}) of the polysulfides on MoC (111) or graphene substrate was calculated as $E_{ads} = E(system) - E(surface) - E(Li_2S_n)$, where $E(system)$ is the energy of the polysulfides adsorbed on the substrate, $E(surface)$ is the energy of the clean substrate, and $E(Li_2S_n)$ is the energy of the isolated polysulfides. The barriers for Li_2S decomposition on MoC (111) and graphene were calculated with the climbing-image nudged elastic band (CI-NEB) method to evaluate delithiation reaction kinetics.[5, 6]

Supplementary Figures and Tables

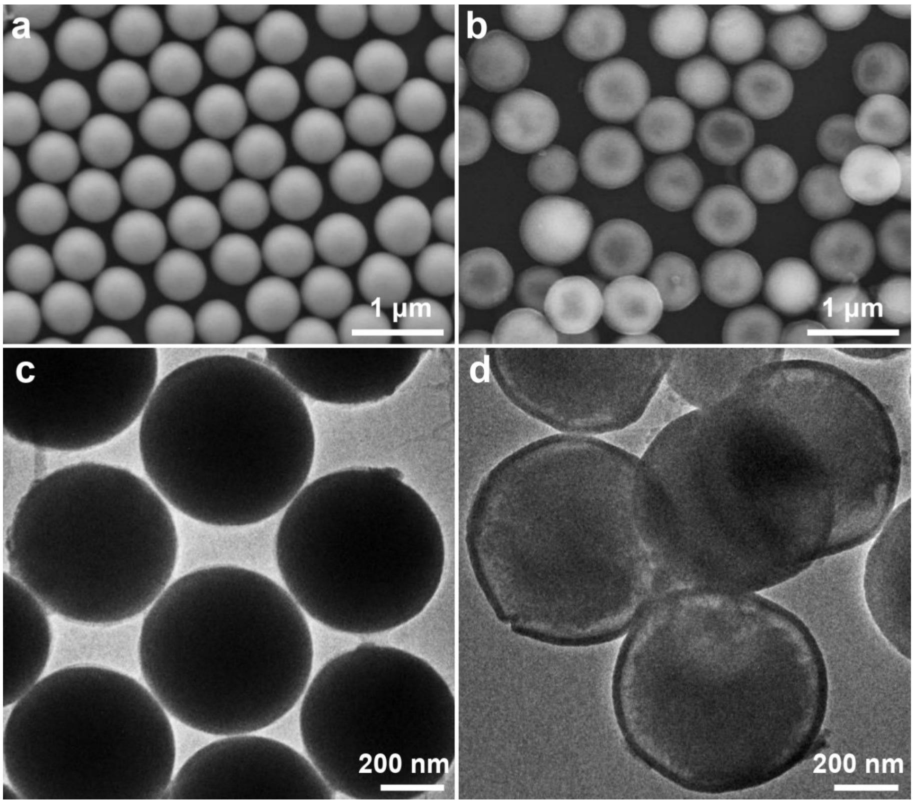

Fig. S1 FESEM and TEM images of (a,c) MoG solid microspheres and (b,d) Mo-PDA CSMSs.

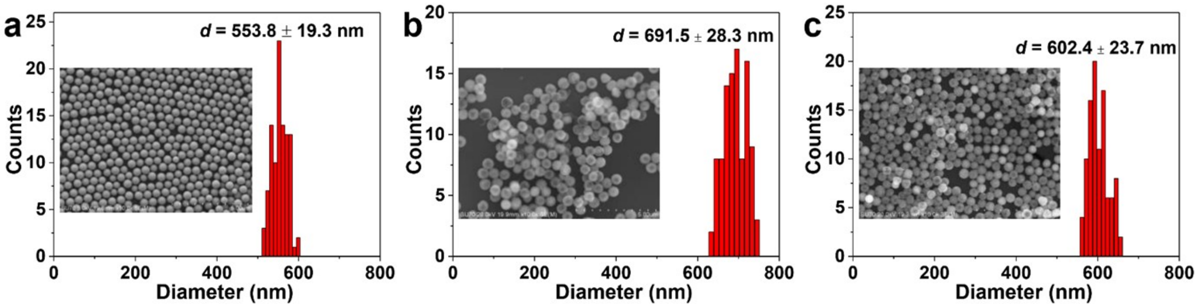

Fig. S2 The statistic histograms of (a) MoG solid microspheres, (b) Mo-PDA CSMSs, and (c) MoC/NC CSMSs according to the FESEM images in the insert.

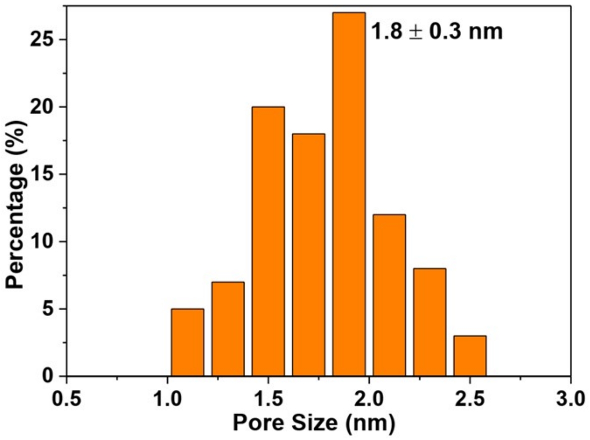

Fig. S3 Statistical size distribution of micropores in the outer shell of MoC/NC CSMSs.

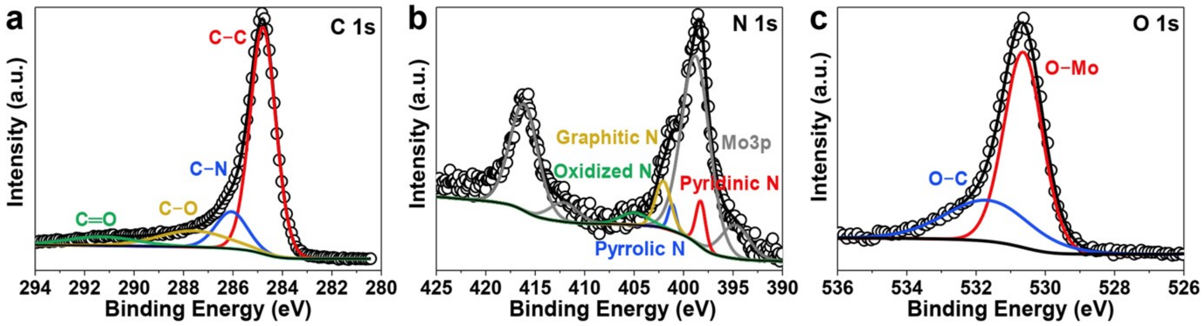

Fig. S4 XPS spectra of (a) C 1s, (b) N 1s, and (c) O 1s of MoC/NC CSMSs.

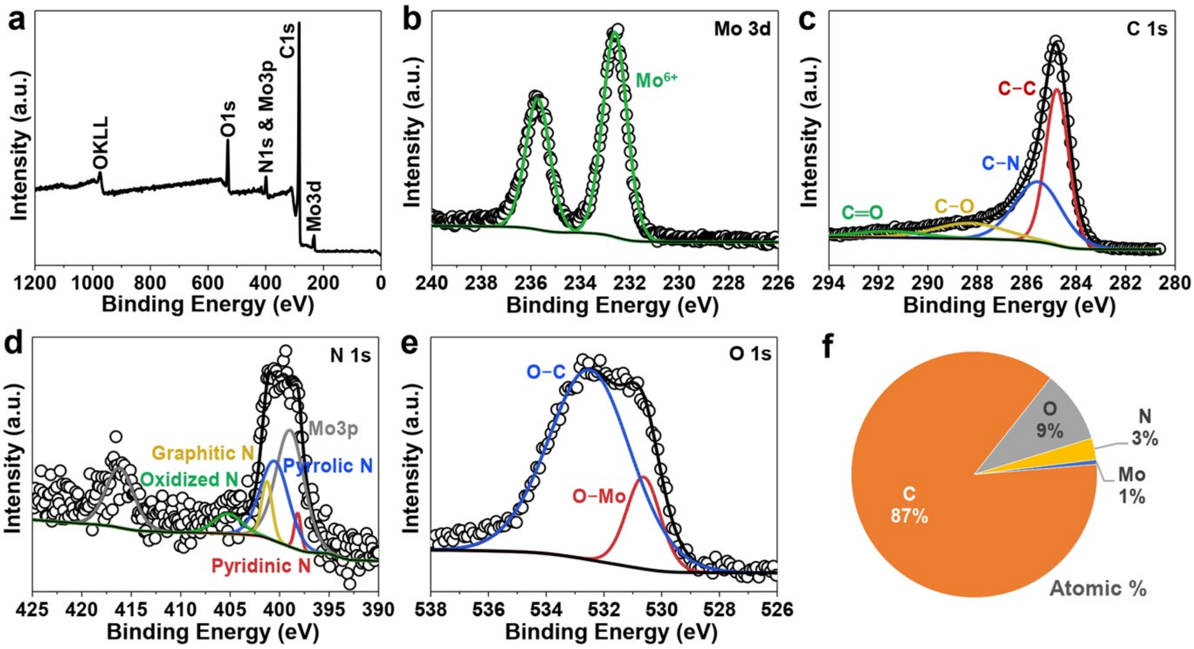

Fig. S5 XPS spectra of NC CSMSs of (a) the survey spectrum, (b) Mo 3d, (c) C 1s, (d) N 1s, and (e) O 1s. (f) The atomic percentage of Mo, C, N, and O.

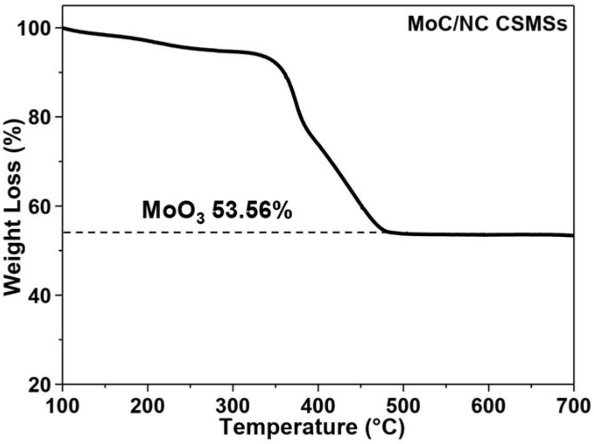

Fig. S6 TGA curve of MoC/NC CSMSs in air atmosphere.

Table S1 The quantitative elemental analysis of MoC/NC CSMSs based on the CHN elemental analysis combined with TGA.

Sample	**C (wt%)**	**H (wt%)**	**N (wt%)**	**Mo (wt%)**	**O (wt%)**
MoC/NC CSMSs	45.1	1.6	2.9	35.7	14.7

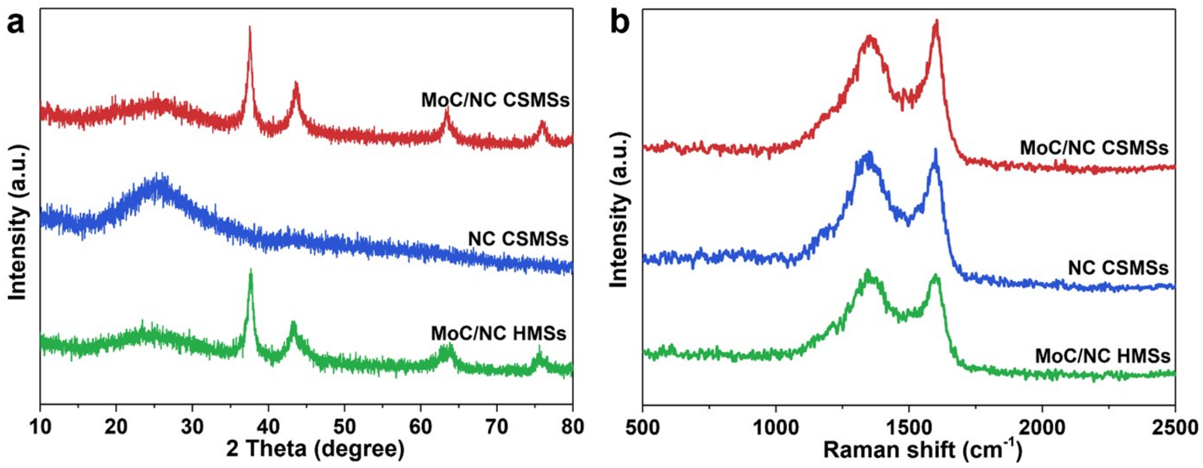

Fig. S7 (a) XRD patterns and (b) Raman results of MoC/NC CSMSs, NC CSMSs, and MoC/NC HMSs. The crystalline sizes of MoC on the MoC/NC CSMSs and MoC/NC HMSs are 7.9 nm and 7.6 nm, respectively, according to the Debye-Scherrer equation.

Table S2 Porosity parameters of the MoC/NC CSMSs and control samples.

Sample	S_{BET} (m^2 g^{-1})	V_{pore} (cm^3 g^{-1})	D_{center} (nm)	$D_{average}$ (nm)
MoC/NC CSMSs	242.2	0.27	1.5/3.7	3.7
NC CSMSs	395.8	0.44	1.6/4.0	3.7
MoC/NC HMSs	160.7	0.15	1.5	2.9

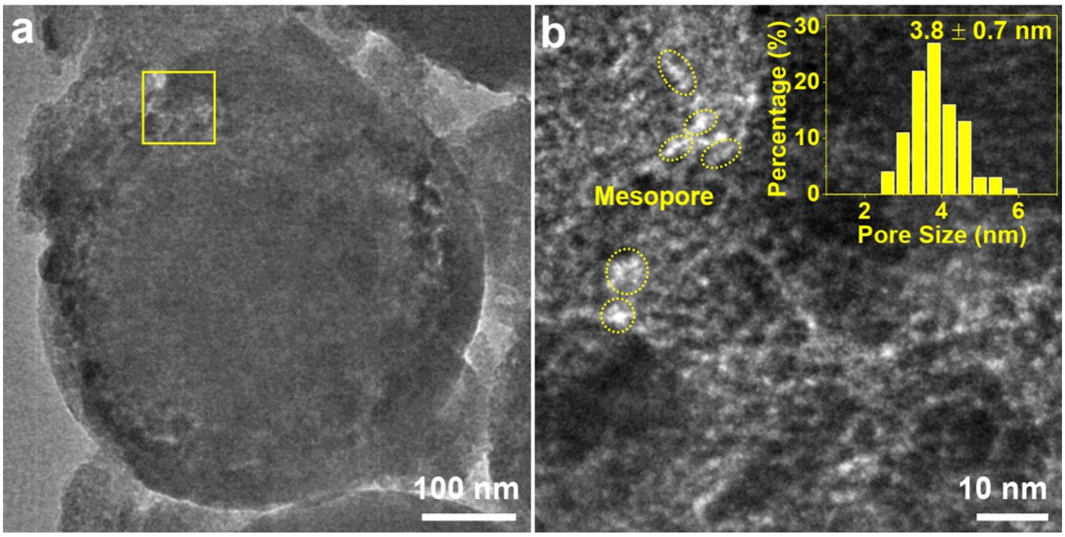

Fig. S8 TEM images of the MoC/NC CSMS with destroyed core-shelled structure. Inset of (b): statistical pore size distribution of mesopores in the edge of the core.

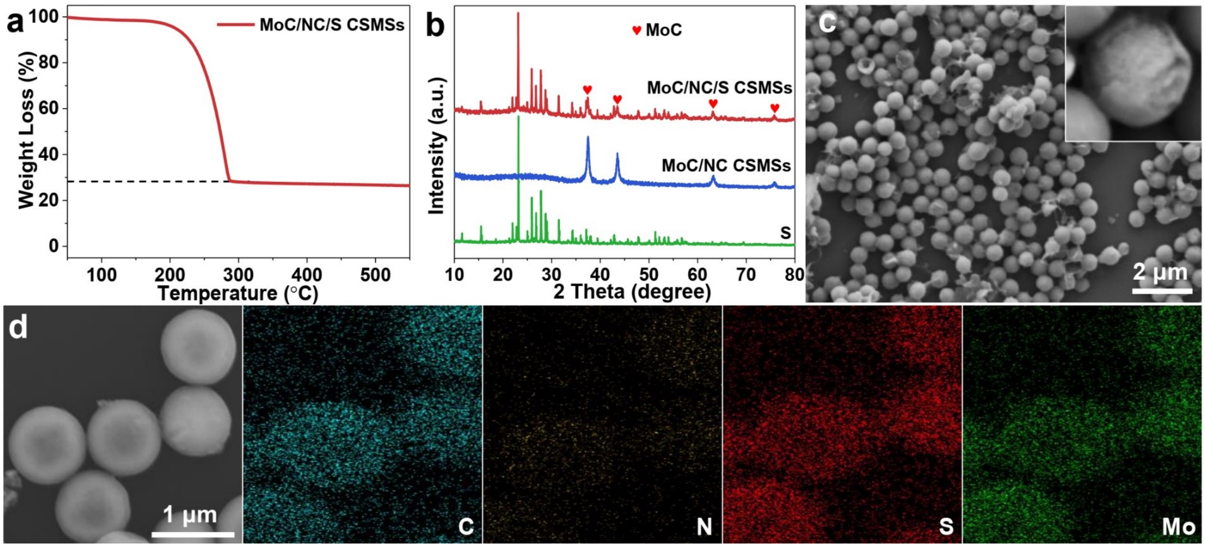

Fig. S9 (a) TGA curve, (b) XRD patterns, (c) FESEM images, and (d) elemental mappings of MoC/NC/S CSMSs.

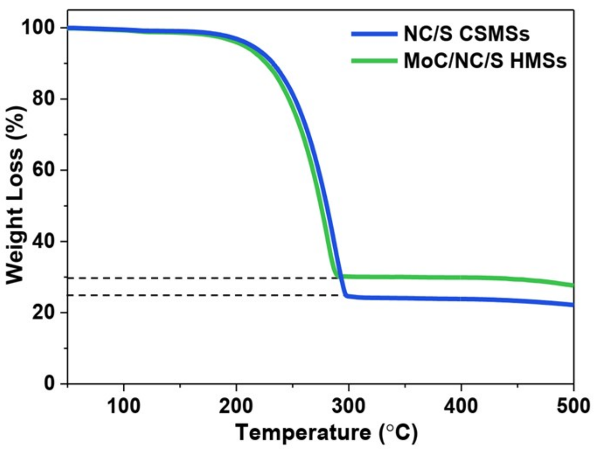

Fig. S10 TGA curves of NC/S CSMSs and MoC/NC/S HMSs in N_2 atmosphere.

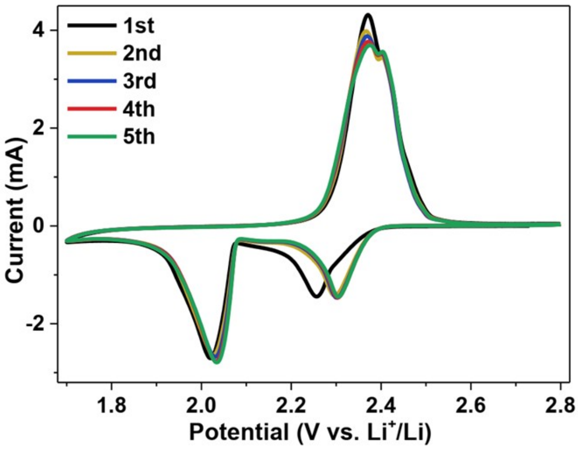

Fig. S11 CV curves of MoC/NC/S CSMSs for the first five cycles at a scan rate of 0.1 mV s^{-1}.

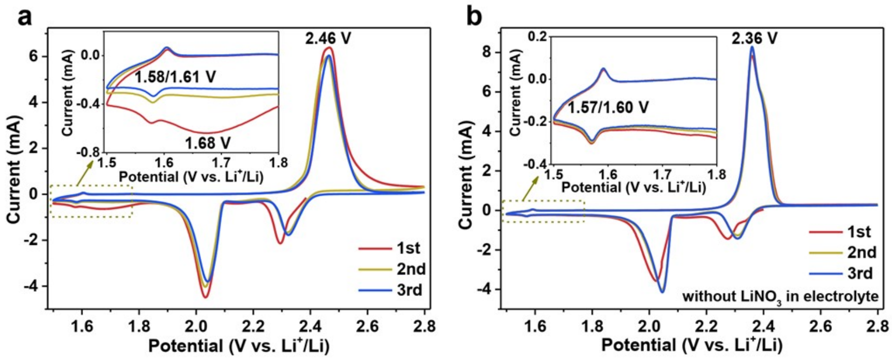

Fig. S12 CV curves of MoC/NC/S CSMSs for the first three cycles at a scan rate of 0.1 mV s^{-1} between 1.5 and 2.8 V with (a) $LiNO_3$-containing electrolyte and (b) $LiNO_3$-free electrolyte.

To investigate the additional discharge at 1.7 V in Fig. 4b, the CV profiles of the MoC/NC/S CSMSs electrode are measured between 1.5 and 2.8 V at a scan rate of 0.1 mV s^{-1}, as shown in Fig. S12a. Except for the redox peaks of sulfur species, an irreversible broad cathodic peak at 1.68 V is observed in the first cycle, which may be associated with the reduction of $LiNO_3$ and Li_2S_2.[7, 8] In the following cycles, this broad peak disappears and a pair of weak redox couples can be detected at 1.58/1.61 V, corresponding to the reversible lithiation/delithiation process of molybdenum oxides on the surface of MoC nanocrystals.[9, 10] When the $LiNO_3$-free electrolyte is used to assemble the Li-S cell, the broad cathodic peak has not been observed in Fig. S12b, which confirms that the irreversible cathodic peak is mainly caused by the reduction of $LiNO_3$ in the electrolyte.

Furthermore, the MoC/NC CSMSs and NC CSMSs without active sulfur species are also prepared as working electrodes to further investigate the electrochemical reaction with potential below 1.7 V. Fig. S13a displays the initial three consecutive CV profiles of the two electrodes. The first cycle of them shows obvious irreversible cathodic waves resulting from the reduction of $LiNO_3$. Moreover, the reduction current with potential below 1.7 V of MoC/NC CSMSs electrode is much higher than that of the NC CSMSs electrode, demonstrating the significant catalytic activity of MoC nanocrystals for the decomposition of $LiNO_3$. In contrast, when the cell using MoC/NC CSMSs as a working electrode is assembled with $LiNO_3$-free electrolyte, this irreversible cathodic wave disappears and the reduction current is distinctly reduced, while the redox couple at 1.57/1.59 V can be still detected (Fig. S13b).

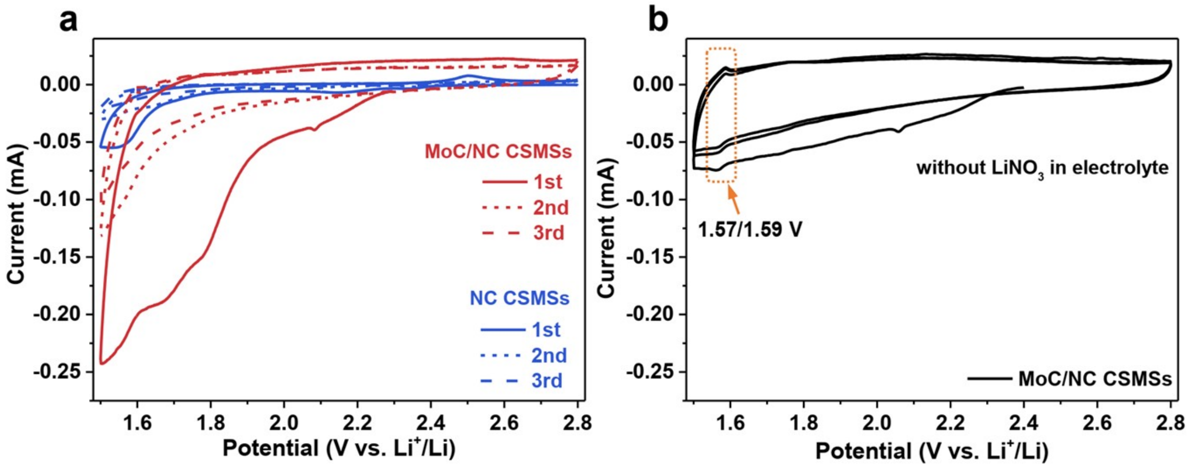

Fig. S13 (a) CV curves of MoC/NC CSMSs and NC CSMSs for the first three cycles at a scan rate of 0.1 mV s^{-1} between 1.5 and 2.8 V with $LiNO_3$-containing electrolyte. (b) CV curves of MoC/NC CSMSs for the first three cycles with $LiNO_3$-free electrolyte.

Therefore, the increase of cathodic current of MoC/NC/S CSMSs electrode around 1.7 V is mainly attributed to the irreversible reduction of $LiNO_3$. Close inspection of the CV curves from 1.7 to 1.9 V in Fig. 4b, the additional discharge at 1.7 V can be observed on all three electrodes, while the MoC/NC/S CSMSs electrode exhibits the highest reduction current, because of the excellent catalytic activity of MoC/NC CSMSs host owing to the synergistic effect of structural advantage of CSMSs and the compositional advantage of MoC nanocrystals. However, this irreversible reduction of $LiNO_3$ lowers the kinetics of the subsequent redox reaction (more severe polarization occurred during the oxidation process in Fig. S12a). Thus, the discharge cutoff voltage at 1.8 V is used in galvanostatic discharge/charge measurements for a long cycle life in this work.

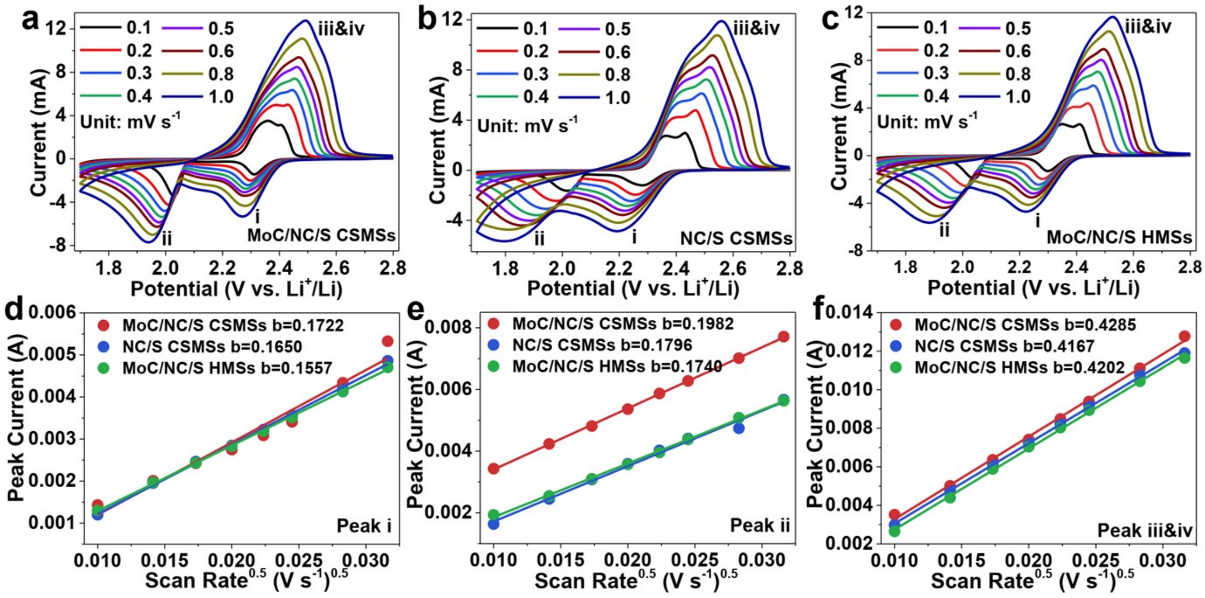

Fig. S14 CV curves at different scan rates of (a) MoC/NC/S CSMSs, (b) NC/S CSMSs and (c) MoC/NC/S HMSs. Anodic peaks of iii and iv are integrated as the scan rate increases. Linear fits of CV peak current depend on the square root of the scan rates in (d) peak i, (e) peak ii, and (f) peak iii&iv.

A series of CV measurements at different scan rates were used to calculate Li-ions diffusion coefficients (D_{Li}) according to the following Randles-Sevcik equation[11-13]

$$I_{peak} = 2.69 \times 10^5 n^{1.5} A D_{Li}^{0.5} \nu^{0.5} C_{Li} \tag{1}$$

where I_{peak} is the peak current (A), n is the number of transferred electrons, A is the electrode area (1.13 cm^2), ν is the scan rate(V s^{-1}), and C_{Li} is the concentration of Li-ions in the electrolyte (1.3068×10^{-3} mol mL^{-1}).

Table S3 The Li-ion diffusion coefficients of MoC/NC/S CSMSs, NC/S CSMSs, and MoC/NC/S HMSs electrodes obtained from the CV measurements.

Electrode	**Peak i (cm^2 s^{-1})**	**Peak ii (cm^2 s^{-1})**	**Peak iii&iv (cm^2 s^{-1})**
MoC/NC/S CSMSs	1.50×10^{-6}	7.38×10^{-8}	1.45×10^{-7}
NC/S CSMSs	1.38×10^{-6}	6.06×10^{-8}	1.38×10^{-7}
MoC/NC/S HMSs	1.23×10^{-6}	5.69×10^{-8}	1.4×10^{-7}

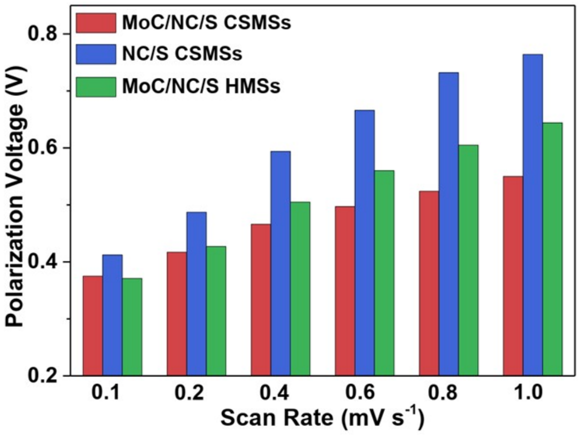

Fig. S15 The polarization voltages (the potential gap between $E_{peak\ ii}$ and $E_{peak\ iii\&iv}$) of MoC/NC/S CSMSs, NC/S CSMSs, and MoC/NC/S HMSs electrodes at different scan rates.

Table S4 Comparisons of the overall performance of the MoC/NC/S CSMSs electrode and its counterparts for Li-S batteries.

Sulfur host material	**Rate performance**							**Cycling performance at 0.2 C for 100 cycles**			**Cycling performance at 1 C for 500 cycles**		
	0.1 C	**0.2 C**	**0.5 C**	**1 C**	**2 C**	**5 C**	**Capacity reversible at 0.2 C (mAh g^{-1})**	**Capacity initial (mAh g^{-1})**	**Capacity retention (mAh g^{-1})**	**Decay rate (%)**	**Capacity initial (mAh g^{-1})**	**Capacity retention (mAh g^{-1})**	**Decay rate (%)**
MoC/NC CSMSs	1370.3 (100%)	1255.6 (91.6%)	1104.5 (80.6%)	1003.3 (73.2%)	856.5 (62.5%)	645.9 (47.1%)	1139.0 (90.7%)	1215.4 (100%)	1077.7 (88.7%)	0.113	963.0 (100%)	798.3 (82.9%)	0.034
NC CSMSs	978.1 (100%)	966.2 (98.8%)	875.6 (89.5%)	759.5 (77.7%)	653.4 (66.8%)	293.3 (30.0%)	936.8 (97.0%)	932.2 (100%)	945.9 (101.5%)	0	699.8 (100%)	616.4 (88.1%)	0.024
MoC/NC HMSs	1256.2 (100%)	1172.4 (93.3%)	1023.7 (81.5%)	874.9 (69.6%)	272.1 (21.7%)	168.4 (13.4%)	1017.2 (86.8%)	1134.1 (100%)	964.5 (85.0%)	0.150	906.6 (100%)	597.3 (65.9%)	0.068

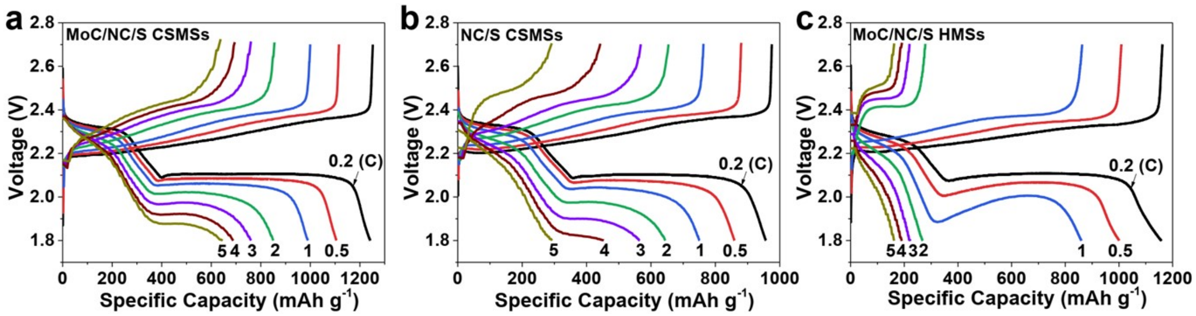

Fig. S16 Charge/discharge curves at different rates of (a) MoC/NC/S CSMSs, (b) NC/S CSMSs and (c) MoC/NC/S HMSs.

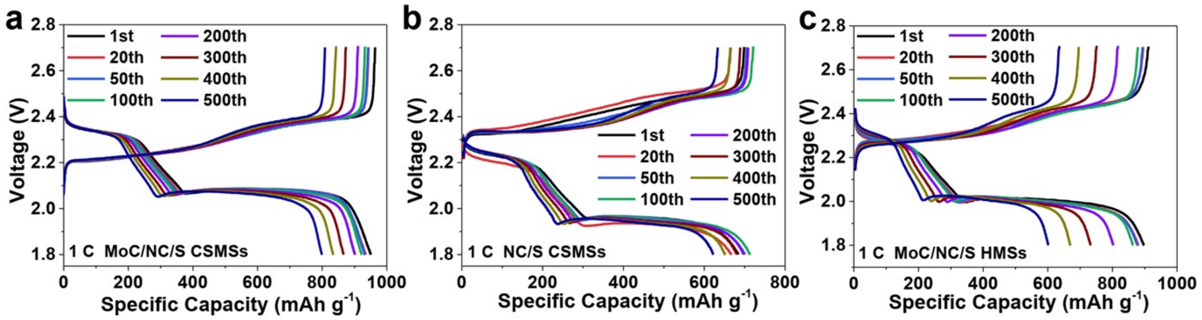

Fig. S17 Charge/discharge curves at different cycles at 1 C of (a) MoC/NC/S CSMSs, (b) NC/S CSMSs and (c) MoC/NC/S HMSs.

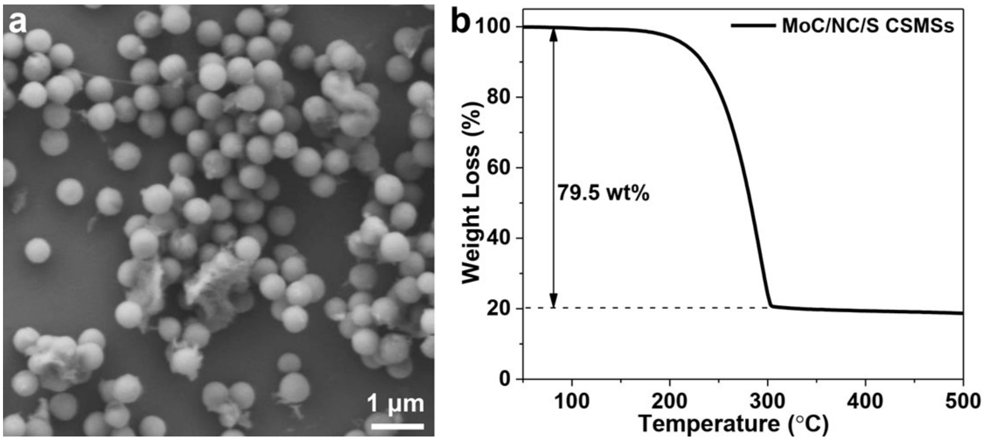

Fig. S18 (a) SEM image and (b) TGA curve of the MoC/NC/S CSMSs with 79.5 wt% sulfur loading.

The sulfur content in the cathode should be as high as possible, to obtain a high energy density. Thus, the MoC/NC/S CSMSs composites with sulfur content up to 79.5 wt% are prepared (Fig. S18). In addition, the cathode slurry is fabricated by mixing 77 wt% MoC/NC/S CSMSs, 15 wt% carbon black, and 8 wt% binders. Whereupon, the sulfur content in the cathode is up to 61.2 wt%.

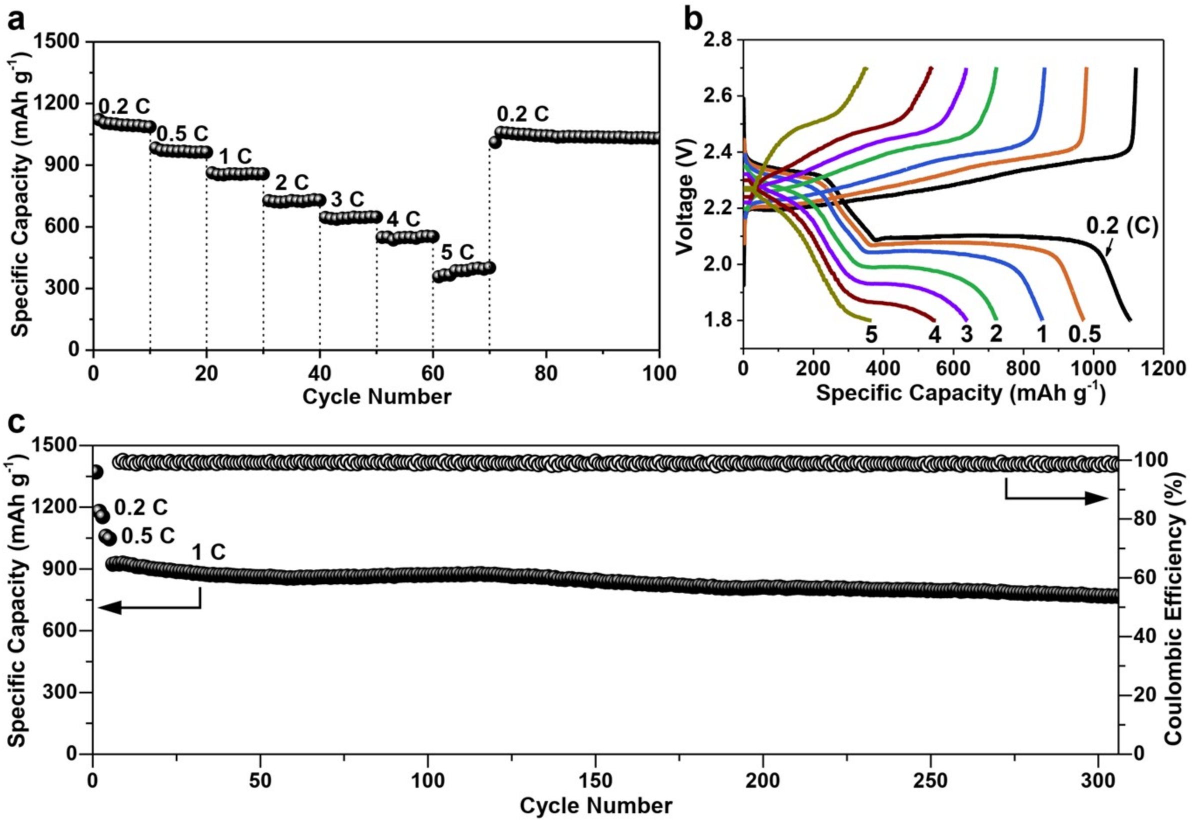

Fig. S19 Electrochemical performance of the MoC/NC/S CSMSs electrode with 79.5 wt% sulfur loading. (a) Rate performance. (b) Charge/discharge profiles at different rates. (c) Cycling performance at 1 C.

The rate performance of MoC/NC/S CSMSs cathode with 61.2 wt% sulfur content is evaluated at current rates from 0.2 to 5 C in Fig. S19a,b. The discharge capacities reach 1105.5, 972.6, 854.0, 722.2, 640.5, 549.6, 366.1 mAh g^{-1} at 0.2, 0.5, 1, 2, 3, 4, and 5 C, respectively, and the corresponding charge/discharge curves deliver a stable discharge plateau even at the current increased to 4 C (Fig. S19b). Subsequently, the discharge capacity reaches 1059.1 mAh g^{-1} when the current rate is decreased back to 0.2 C, demonstrating high specific capacities and good rate capability at current rates from 0.2 to 4 C. As for the long-term stability at 1 C (Fig. S19c), the MoC/NC/S CSMSs cathode with 61.2 wt% sulfur content delivers high initial discharge capacity of 922.5 mAh g^{-1} and presents low capacity decay rate (0.056 % per cycle) for 300 cycles. These results confirm that the cooperation of CSMSs structure and MoC/NC composition lead to a good performance of the MoC/NC/S CSMSs cathode with sulfur content up to 61.2 wt%.

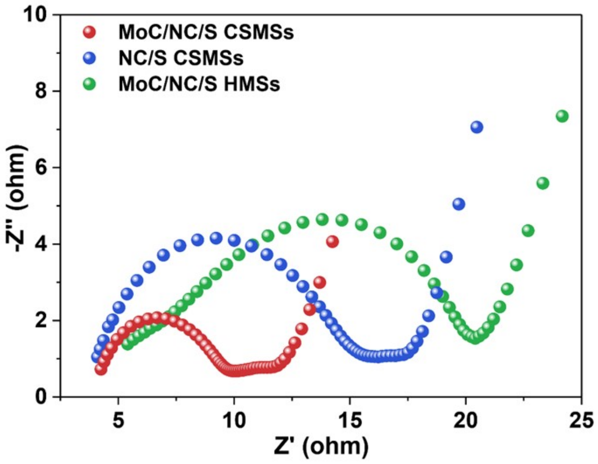

Fig. S20 Nyquist impedance plots after 500 cycles at 1 C.

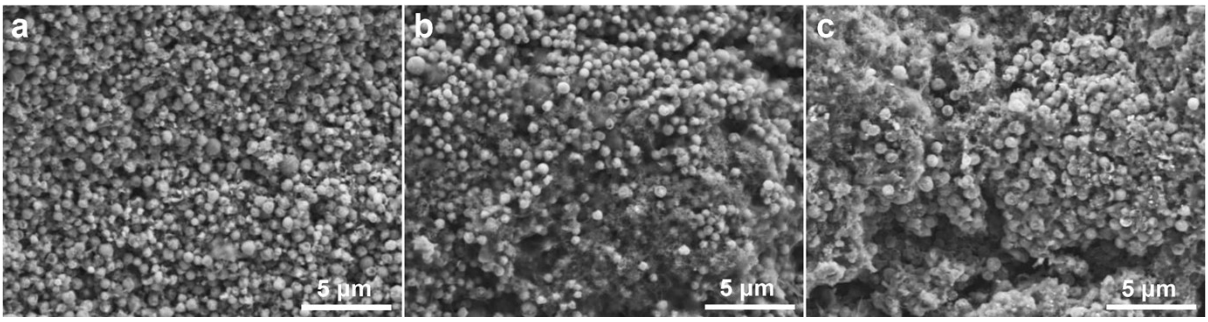

Fig. S21 FESEM images of the cathodes of (a) MoC/NC/S CSMSs, (b) NC/S CSMSs and (c) MoC/NC/S HMSs after 500 cycles at 1 C.

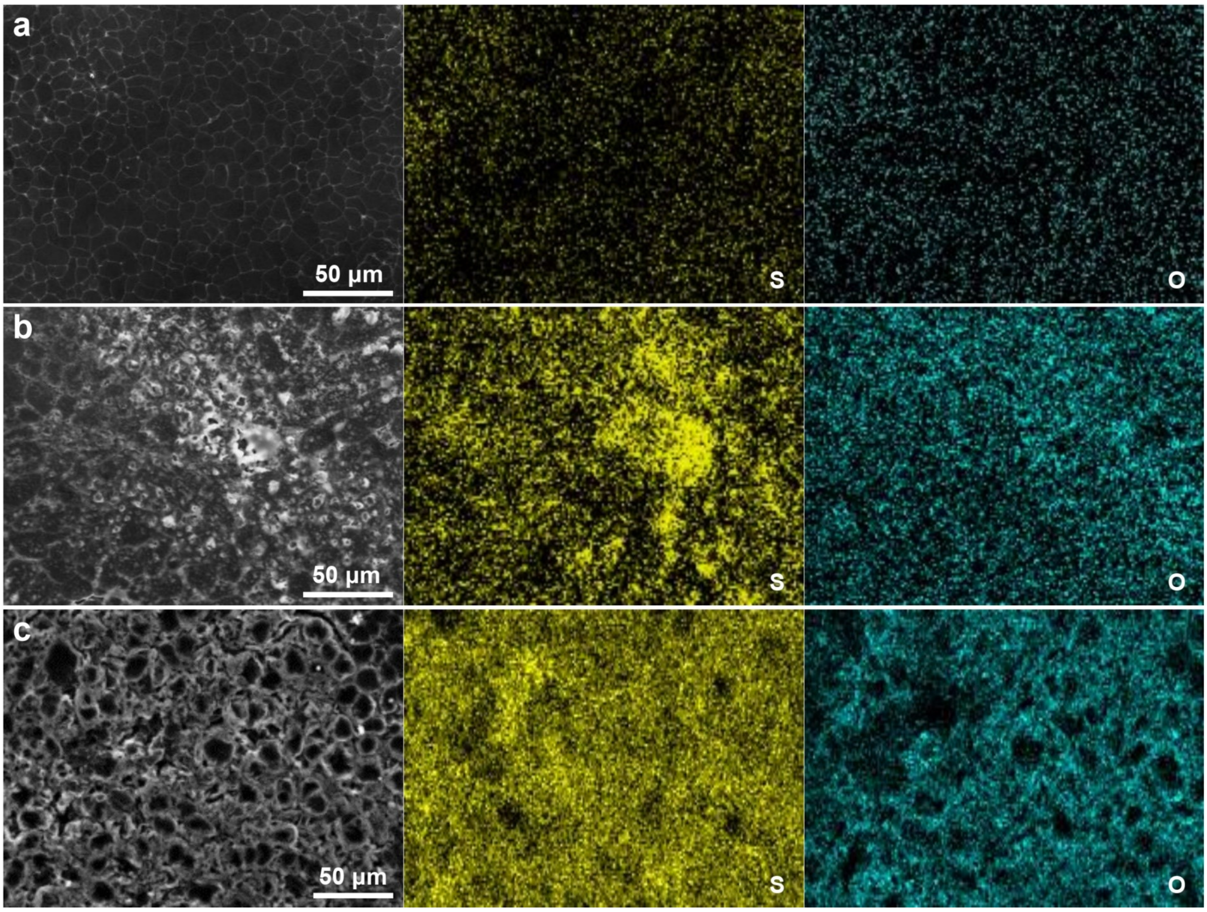

Fig. S22 FESEM images and elemental mappings of the Li anodes after 500 cycles at 1 C with (a) MoC/NC/S CSMSs, (b) NC/S CSMSs, and (c) MoC/NC/S HMSs as cathode, respectively.

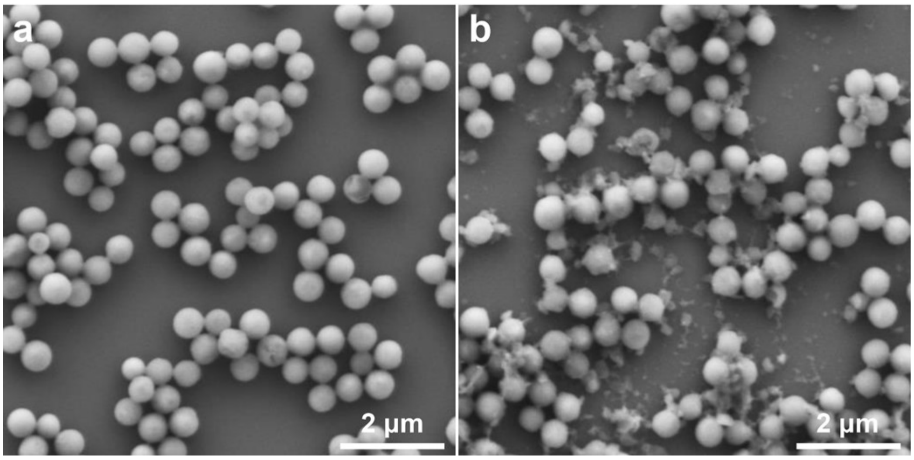

Fig. S23 FESEM images of MoC/NC CSMSs (a) before and (b) after sonication for 5 h using ultrasonic cell crusher (760 W).

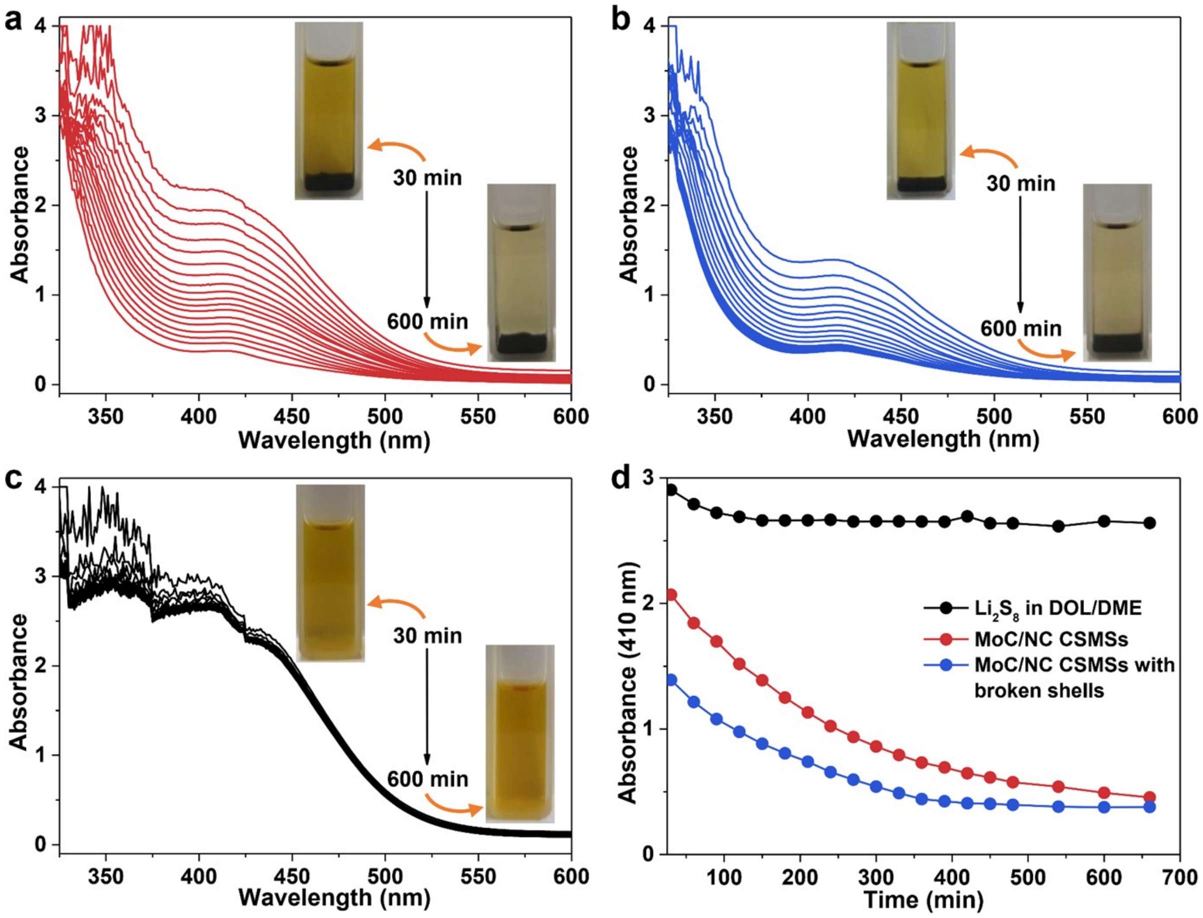

Fig. S24 UV-vis spectra and the photographs of Li_2S_8 in DOL/DME solution (1.5 mM) after being adsorbed at different times by powders of (a) MoC/NC CSMSs, (b) MoC/NC CSMSs with broken shells, and (c) control. (d) The time-dependent absorbance changes at 410 nm.

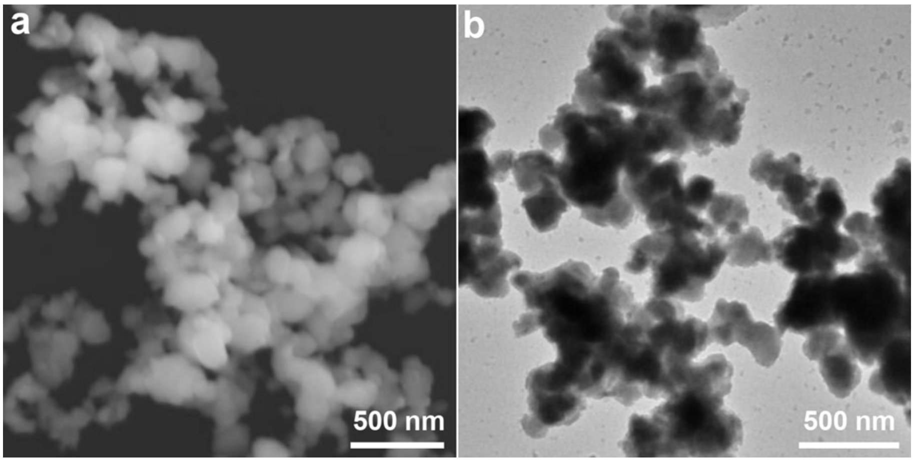

Fig. S25 (a) FESEM image and (b) TEM image of MoC/NC NPs.

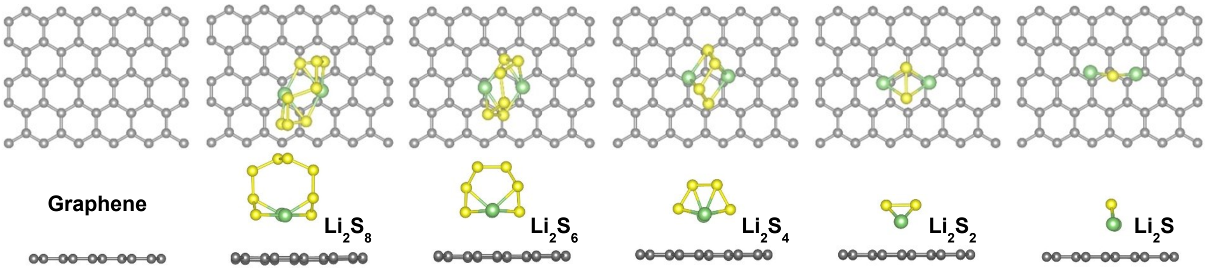

Fig. S26 Optimized geometries of LiPSs adsorption on the surface of graphene.

Table S5 Comparisons the performance of the MoC/NC/S CSMSs electrode in this work with related references.

Electrode	Sulfur content (wt%)	Cycles/Rate	Initial/Retentive capacity (mAh g^{-1})	Decay rate (%)	Rate capability	Ref.
MoC/NC/S CSMSs	73	500/1C	963.0/798.3	0.034	856.5/2C 645.9/5C	This work
	80	300/1C	922.5/766.6	0.056	722.2/2C	
HCNCs-2/S	73	300/1C	1196/630	0.158	592/5C	[14]
TI-NHCNS/S	75	1000/1C	747/418	0.044	540/5C	[15]
SDC/TiO$_2$/S	74	1500/0.9C	749/569	0.016	845/0.9C	[16]
Bi$_2$S$_3$-PPy HSs/S	64	500/1C	1180/729	0.076	515/3C	[17]
Co$_9$S$_8$@CNTs/S	69	1000/2C	1017.4/560.6	0.045	676.7/10C	[18]
MoC@MoO$_x$-CFF/Li$_2$S$_6$	51	200/0.2C	980/800	0.092	--	[19]
β-Mo$_2$C NRs-S	67	500/1C	968/669	0.062	786/2C	[20]
β-Mo$_2$C/S	70	300/0.2C	--/789.4	--	660/5C	[21]
η-MoC@N-CNF/Li$_2$S$_6$	55	350/1C	911/644	0.084	799/2C	[22]
β-Mo$_2$C-C NOs@S	72	600/1C	1050/762	0.046	337/5C	[23]
β-Mo$_2$C/C@C(2)-S	77	300/1C	800/652	0.062	--/2C	[24]

References

1 Y. Wang, L. Yu and X. W. Lou, *Angew. Chem. Int. Ed.*, 2016, **55**, 14668-14672.

2 G. Kresse and J. Furthmüller, *Comput. Mater. Sci.*, 1996, **6**, 15-50.

3 G. Kresse and J. Furthmüller, *Phys. Rev. B*, 1996, **54**, 11169-11186.

4 J. P. Perdew, K. Burke and M. Ernzerhof, *Phys. Rev. Lett.*, 1996, **77**, 3865-3868.

5 Z. Du, X. Chen, W. Hu, C. Chuang, S. Xie, A. Hu, W. Yan, X. Kong, X. Wu, H. Ji and L.-J. Wan, *J. Am. Chem. Soc.*, 2019, **141**, 3977-3985.

6 G. Henkelman, B. P. Uberuaga and H. Jónsson, *J. Chem. Phys.*, 2000, **113**, 9901-9904.

7 K. Mi, Y. Jiang, J. Feng, Y. Qian and S. Xiong, *Adv. Funct. Mater.*, 2016, **26**, 1571-1579.

8 S. S. Zhang, *J. Electrochem. Soc.*, 2012, **159**, A920-A923.

9 C. Wang, L. Sun, F. Zhang, X. Wang, Q. Sun, Y. Cheng and L. Wang, *Small*, 2017, **13**, 1701246.

10 Q. Gao, X. Zhao, Y. Xiao, D. Zhao and M. Cao, *Nanoscale*, 2014, **6**, 6151-6157.

11 B. Ding, C. Yuan, L. Shen, G. Xu, P. Nie and X. Zhang, *Chem. Eur. J.*, 2013, **19**, 1013-1019.

12 Y. Yang, G. Zheng and Y. Cui, *Chem. Soc. Rev.*, 2013, **42**, 3018-3032.

13 W. G. Lim, C. Jo, A. Cho, J. Hwang, S. Kim, J. W. Han and J. Lee, *Adv. Mater.*, 2019, **31**, 1806547.

14 M. Chen, Z. Su, K. Jiang, Y. Pan, Y. Zhang and D. Long, *J. Mater. Chem. A*, 2019, **7**, 6250-6258.

15 Z. Yu, M. Liu, D. Guo, J. Wang, X. Chen, J. Li, H. Jin, Z. Yang, X. Chen and S. Wang, *Angew. Chem. Int. Ed.*, 2020, **59**, 6406-6411.

16 W. Wu, J. Pu, J. Wang, Z. Shen, H. Tang, Z. Deng, X. Tao, F. Pan and H. Zhang, *Adv. Energy Mater.*, 2018, **8**, 1702373.

17 B. Long, Z. Qiao, J. Zhang, S. Zhang, M.-S. Balogun, J. Lu, S. Song and Y. Tong, *J. Mater. Chem. A*, 2019, **7**, 11370-11378.

18 J. Zhou, X. Liu, J. Zhou, H. Zhao, N. Lin, L. Zhu, Y. Zhu, G. Wang and Y. Qian, *Nanoscale Horiz.*, 2019, **4**, 182-189.

19 R. Fang, S. Zhao, Z. Sun, D.-W. Wang, R. Amal, S. Wang, H.-M. Cheng and F. Li, *Energy Storage Mater.*, 2018, **10**, 56-61.

20 Z. Wang, J. Liu, L. Sun, Y. Zhang, Q. Fu, H. Xie and H. Sun, *Chem. Eur. J.*, 2018, **24**, 14154-14161.

21 X. Zeng, X. Gao, G. Li, M. Sun, Z. Lin, M. Ling, J. Zheng and C. Liang, *J. Mater. Chem. A*, 2018, **6**, 17142-17147.

22 H. Shi, Z. Sun, W. Lv, S. Wang, Y. Shi, Y. Zhang, S. Xiao, H. Yang, Q.-H. Yang and F. Li, *J. Mater. Chem. A*, 2019, **7**, 11298-11304.

23 G. Chen, Y. Li, W. Zhong, F. Zheng, J. Hu, X. Ji, W. Liu, C. Yang, Z. Lin and M. Liu, *Energy Storage Mater.*, 2020, **25**, 547-554.

24 Z. Wang, X. Xu, Z. Liu, S. Ji, S. O. Ahmed Idris and J. Liu, *Electrochim. Acta*, 2020, **332**, 135482.